Title
Targeting the DNA Repair Pathway in Ewing Sarcoma

Journal
Cell Reports, 9(3)

ISSN
2639-1856

Authors
Stewart, Elizabeth
Goshorn, Ross
Bradley, Cori
et al.

Publication Date
2014-11-01

DOI
10.1016/j.celrep.2014.09.028

Peer reviewed

Report

Cell Reports

Targeting the DNA Repair Pathway in Ewing Sarcoma

Graphical Abstract

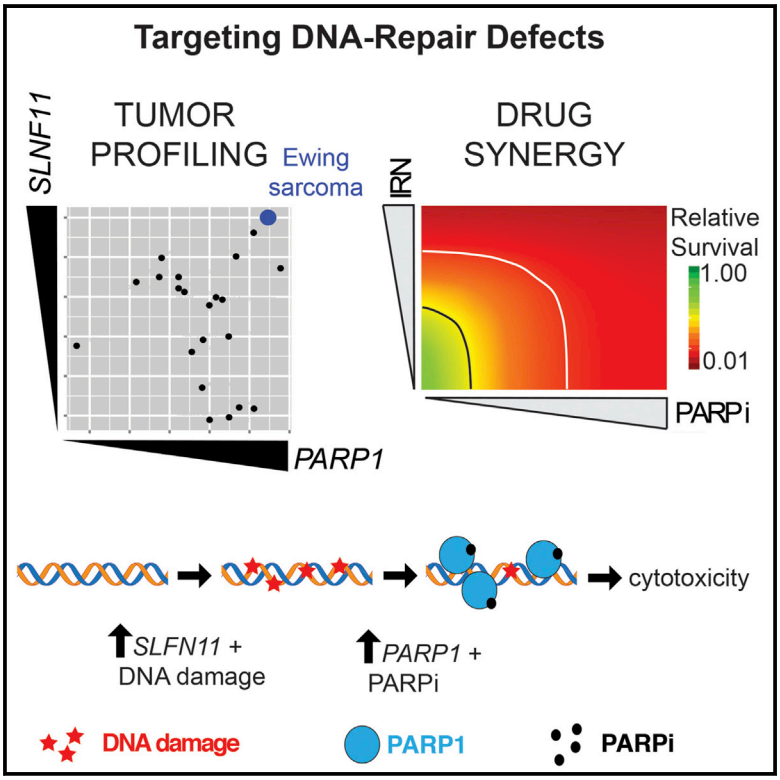

Highlights

Ewing sarcoma cells are defective in DNA damage repair

DNA damage potentiates the effect of PARP inhibitors in Ewing sarcoma cells

PARP inhibitors might be combined with irinotecan and temozolomide for EWS treatment

Authors

Elizabeth Stewart, Ross Goshorn, ..., Anang A. Shelat, Michael A. Dyer

Correspondence

anang.shelat@stjude.org (A.A.S.), michael.dyer@stjude.org (M.A.D.)

In Brief

Stewart et al. now find that Ewing sarcoma cells are defective in DNA damage repair and sensitive to PARP inhibitors. The schedule of irinotecan used in pediatric patients is well tolerated and can potentiate PARP-inhibitor-mediated killing of Ewing sarcoma cells in vivo. These data raise the possibility that PARP inhibitors may be combined with irinotecan and temozolomide for the treatment of Ewing sarcoma.

Stewart et al., 2014, Cell Reports 9, 829–840
November 6, 2014 ©2014 The Authors
http://dx.doi.org/10.1016/j.celrep.2014.09.028

Cell Reports
Report

Targeting the DNA Repair Pathway in Ewing Sarcoma

Elizabeth Stewart,[1] Ross Goshorn,[1] Cori Bradley,[1] Lyra M. Griffiths,[1] Claudia Benavente,[1] Nathaniel R. Twarog,[2] Gregory M. Miller,[2] William Caufield,[3] Burgess B. Freeman III,[3] Armita Bahrami,[4] Alberto Pappo,[5] Jianrong Wu,[6] Amos Loh,[1] Åsa Karlström,[1] Chris Calabrese,[7] Brittney Gordon,[7] Lyudmila Tsurkan,[2] M. Jason Hatfield,[2] Philip M. Potter,[2] Scott E. Snyder,[2] Suresh Thiagarajan,[8] Abbas Shirinifard,[8] Andras Sablauer,[8] Anang A. Shelat,[2,*] and Michael A. Dyer[1,9,*]
[1]Department of Developmental Neurobiology, St. Jude Children's Research Hospital, Memphis, TN 38105, USA
[2]Department of Chemical Biology and Therapeutics, St. Jude Children's Research Hospital, Memphis, TN 38105, USA
[3]Preclinical Pharmacokinetics Shared Resource, St. Jude Children's Research Hospital, Memphis, TN 38105, USA
[4]Department of Pathology, St. Jude Children's Research Hospital, Memphis, TN 38105, USA
[5]Department of Oncology, St. Jude Children's Research Hospital, Memphis, TN 38105, USA
[6]Department of Biostatistics, St. Jude Children's Research Hospital, Memphis, TN 38105, USA
[7]Animal Imaging Shared Resource, St. Jude Children's Research Hospital, Memphis, TN 38105, USA
[8]Department of Radiological Sciences, St. Jude Children's Research Hospital, Memphis, TN 38105, USA
[9]Howard Hughes Medical Institute, Chevy Chase, MD 20815, USA
*Correspondence: anang.shelat@stjude.org (A.A.S.), michael.dyer@stjude.org (M.A.D.)
http://dx.doi.org/10.1016/j.celrep.2014.09.028

SUMMARY

Ewing sarcoma (EWS) is a tumor of the bone and soft tissue that primarily affects adolescents and young adults. With current therapies, 70% of patients with localized disease survive, but patients with metastatic or recurrent disease have a poor outcome. We found that EWS cell lines are defective in DNA break repair and are sensitive to PARP inhibitors ($PARP_i$s). $PARP_i$-induced cytotoxicity in EWS cells was 10- to 1,000-fold higher after administration of the DNA-damaging agents irinotecan or temozolomide. We developed an orthotopic EWS mouse model and performed pharmacokinetic and pharmacodynamic studies using three different $PARP_i$s that are in clinical development for pediatric cancer. Irinotecan administered on a low-dose, protracted schedule previously optimized for pediatric patients was an effective DNA-damaging agent when combined with $PARP_i$s; it was also better tolerated than combinations with temozolomide. Combining $PARP_i$s with irinotecan and temozolomide gave complete and durable responses in more than 80% of the mice.

INTRODUCTION

Ewing sarcoma (EWS) is the second most common bone tumor in children and adolescents; approximately 250 new cases are diagnosed each year in the US (Howlader et al., 2013). Most EWS tumors have a translocation involving the *EWS* gene on chromosome 22 and the *FLI* gene on chromosome 11 (Delattre et al., 1992). The *EWS-FLI* translocation is an important driver of tumorigenesis in EWS (Lessnick and Ladanyi, 2012). Patients with recurrent or metastatic disease have a poor outcome (Granowetter et al., 2009; Stahl et al., 2011). Recent clinical trials in relapsed disease have shown that the combination of irinotecan (IRN) and temozolomide (TMZ) is active in EWS, and these drugs are now used in combination with other agents such as temsirolimus (Bagatell et al., 2011).

EWS cell lines are sensitive to the poly-ADP ribose polymerase inhibitor ($PARP_i$) olaparib, and this sensitivity is selective for EWS cell lines (Brenner et al., 2012; Garnett et al., 2012). Olaparib sensitivity depends on the *EWS-FLI* translocation, suggesting a direct mechanistic connection between PARP inhibition by olaparib and the mechanism of transformation by EWS-FLI (Brenner et al., 2012; Garnett et al., 2012). Brenner et al. also showed that the EWS-FLI1 fusion protein interacts with PARP1 and proposed a positive-feedback loop involving both proteins (Brenner et al., 2012). High levels of PARP1 expression are correlated with increased sensitivity to $PARP_i$s (Byers et al., 2012; Pettitt et al., 2013; Bajrami et al., 2014), consistent with a "trapping" mechanism whereby the inhibitor acts as a poison to stabilize a PARP-DNA complex (Murai et al., 2012). Furthermore, EWS cell lines express high levels of Schlafen-11 (SLFN11), a putative DNA/RNA helicase whose expression is positively correlated with increased sensitivity to Topoisomerase I inhibitors ($Topo1_i$) and other DNA-damaging agents, but not protein kinase inhibitors or tubulin poisons (Barretina et al., 2012; Zoppoli et al., 2012). For *BRCA*-deficient breast cancer and ovarian cancer, $PARP_i$s are combined with DNA-damaging agents to potentiate selective tumor-cell killing (Ashworth, 2008; Bryant et al., 2005; Farmer et al., 2005; Fong et al., 2009; Tutt et al., 2005).

In this study, we tested the cytotoxic activity and in vivo efficacy of three different $PARP_i$s (BMN-673, olaparib, veliparib) in combination with IRN and TMZ. Both TMZ and IRN potentiated $PARP_i$-mediated killing of EWS cells, but at least a 1,000-fold higher concentration of TMZ was required to achieve the same level of potentiation as that achieved with IRN. We performed in vivo plasma and tumor pharmacokinetic (PK) experiments in parallel with pharmacodynamics (PD) studies for each $PARP_i$ to determine the murine-equivalent dose (MED) and whether sufficient levels of drug can be reached in the tumor to mediate tumor-cell killing. The data were used to design preclinical phase I,

II, and III studies to test 15 drug combinations incorporating all three PARP$_i$s with IRN, TMZ, or both.

RESULTS

EWS Cells Are Defective in DNA Break Repair

An analysis of the Cancer Cell Line Encyclopedia indicates that EWS behaves as an outlier and shows high levels of both *PARP1* and *SLNF11* compared to other cancers, including osteosarcoma (OS), another form of bone cancer (Barretina et al., 2012). Because high levels of *SLFN11* expression can increase sensitivity to DNA-damaging agents (Zoppoli et al., 2012), we reasoned that EWS might be deficient in DNA damage repair. We performed quantitative PCR (qPCR) using TaqMan probes for 46 DNA repair genes and confirmed the downregulation of *BRCA1*, *GEN1*, and *ATM*; in addition, several other genes in EWS cell lines were downregulated relative to their levels in OS cell lines and OS orthotopic xenografts (Figures S1). Gene expression array data from primary EWS and OS tumors were consistent with our qPCR data and confirmed higher levels of *PARP1* and *SLFN11* in EWS (Table S1).

To monitor DNA damage in individual cells, we performed a single-cell alkali gel electrophoresis (comet) assay using an OS cell line (U2OS) and ES-8 EWS cells (Figure 1A). Thirty minutes after 10 Gy ionizing radiation (IR) exposure, the tail moment significantly increased for both cells (Figures 1B and 1C). However, 11 hr after IR exposure, the tail moment in the OS line was restored to basal levels, but that ES-8 EWS was not (Figures 1B and 1C). To analyze the contribution of PARP, we performed a similar experiment in the presence of olaparib, veliparib, and BMN-673 at two concentrations (1 or 10 μM). At 10 μM olaparib and 1 or 10 μM BMN-673, the basal level of DNA damage after 12 hr of exposure to the PARP$_i$ was elevated in ES-8, especially for BMN-673 (Figures 1D–1G). This DNA repair defect was even more pronounced when the cells were exposed to 10 Gy IR (Figures 1D–1G).

To independently validate these data, we performed γ-H2AX immunostaining analysis on ES-1, ES-6, ES-8, EW-8, U2OS, and SAOS cells. The basal proportion of cells that were γ-H2AX$^+$ and the distribution of γ-H2AX$^+$ foci per nucleus were similar across the EWS and OS cell lines (Figure S1). All cell lines showed rapid γ-H2AX localization to foci with double-strand DNA (dsDNA) breaks after exposure to 5 Gy IR (Figure S1). To determine whether any defect in the repair of the dsDNA breaks occurred after IR exposure, we performed a time course experiment. Cells were exposed to 5 Gy IR, and then, at 5 min, 2 hr, 8 hr, and 24 hr, the proportions of γ-H2AX$^+$ cells (>20 foci/cell) were scored. In the OS cell line, the proportion of γ-H2AX$^+$ decreased at 2 hr after IR exposure; by 8 hr, the cells were indistinguishable from the original cell population. The resolution of γ-H2AX$^+$ foci was significantly slower for the EWS cell line ($p < 0.01$; Figure 1H). To determine whether exposure to PARP$_i$s further delays the repair of IR-induced dsDNA breaks, we performed a similar experiment in the presence of olaparib, veliparib, or BMN-673 (Figure S1). The number of γ-H2AX$^+$ cells was significantly increased at 24 hr after IR exposure in the presence of PARP$_i$s ($p < 0.01$; Figure S1). Together, these data suggest that EWS cell lines are defective in DNA repair.

DNA-Damaging Agent and PARP$_i$ Cytotoxicity in EWS Cells

IRN and TMZ are used in combination to treat recurrent EWS (Casey et al., 2009), and both drugs induce DNA damage through distinct mechanisms (Figure 2A) (Hsiang et al., 1989; Quiros et al., 2010). We performed dose-response experiments measuring the cytotoxicity of SN-38 (the active metabolite of IRN), TMZ, BMN-673, olaparib, and veliparib in eight Ewing sarcoma cell lines (ES-1, ES-4, ES-6, ES-7, ES-8, EW-8, RD-ES, and SK-ES1), three OS cell lines (SAOS2, SAOS2LM7, and U2OS), and five OS xenografts (MAST22, MAST38, OS39R, OS43, and OS45).The EWS cell lines were chosen to reflect diversity in *EWS-FLI1* translocation type, p53 status, and STAG2 status (Supplemental Information). At 72 hr of exposure, EW-8, ES-8, and ES-1 cells were sensitive to BMN-673 and olaparib, and, at 144 hr, all EWS cell lines except ES-6 were sensitive to all three PARP$_i$s (Figures 2B–2E and S2; Table S2), though veliparib activity was marginal. ES-6 cells, which have a nonfunctional *EWS-FLI1* translocation, were reported to be resistant to olaparib at 72 hr but had some sensitivity at later time points in colony assays (Garnett et al., 2012). In our analysis, ES-6 cells were resistant to all three PARP$_i$s at 72 hr and to BMN-673 and veliparib at 144 hr and had significantly lower potency for olaparib and SN-38 compared to other EWS cell lines (Table S2). At 144 hr, all EWS cell lines tested excluding ES-6 had EC_{50} <10 nM for SN-38 and >100 μM for TMZ. In contrast to EWS cells, OS cells showed little sensitivity to any of the compounds tested. Only one compound had an EC_{50} <100 nM: SN-38 in SAOS2 (Table S2).

To determine whether sensitivity to PARP$_i$s depends on the expression of PARP1, we knocked down PARP1 protein in ES-8 cells with a small interfering RNA (siRNA) (Murai et al., 2012) (Figures 2F–2J). For each drug, PARP$_i$ sensitivity was reduced when PARP1 expression was knocked down relative to a control siRNA, consistent with the PARP trapping mechanism (Murai et al., 2012, 2014). Indeed, PARP trapping potential followed the same trend observed in the cytotoxicity assay BMN-673 > olaparib > veliparib (Figure S2).

Development of an Orthotopic EWS Xenograft Model

To generate an EWS orthotopic xenograft, we developed a method for injecting EWS cell lines or primary human tumor cells into the bone marrow of the femur of immunocompromised mice (Supplemental Information). Briefly, cells are resuspended in Matrigel at 100,000 cells/μl and drawn up in a Hamilton syringe with a 25 G needle. The patella and ligaments of the knee are laterally displaced, and the needle is inserted into the intercondylar fossa by using a closed technique (Figures 3A–3F). Early signs of engraftment include periosteal elevation on X-ray images, followed by local tumor cell invasion, and hair-on-end appearance (Figure 3G), as seen in patients with EWS. The soft-tissue features of EWS orthotopic xenografts can be visualized by MRI (Figure 3H), and tumor calcification and accompanying alterations in femoral architecture can be monitored via micro-CT (Figure 3I). We also tested two positron emission tomography (PET) tracers (F^{18}-deoxyglucose and C^{11}-methionine); C^{11}-methionine provided superior sensitivity and signal-to-noise for the orthotopic EWS xenografts (Figures 3J–3M; data not shown).

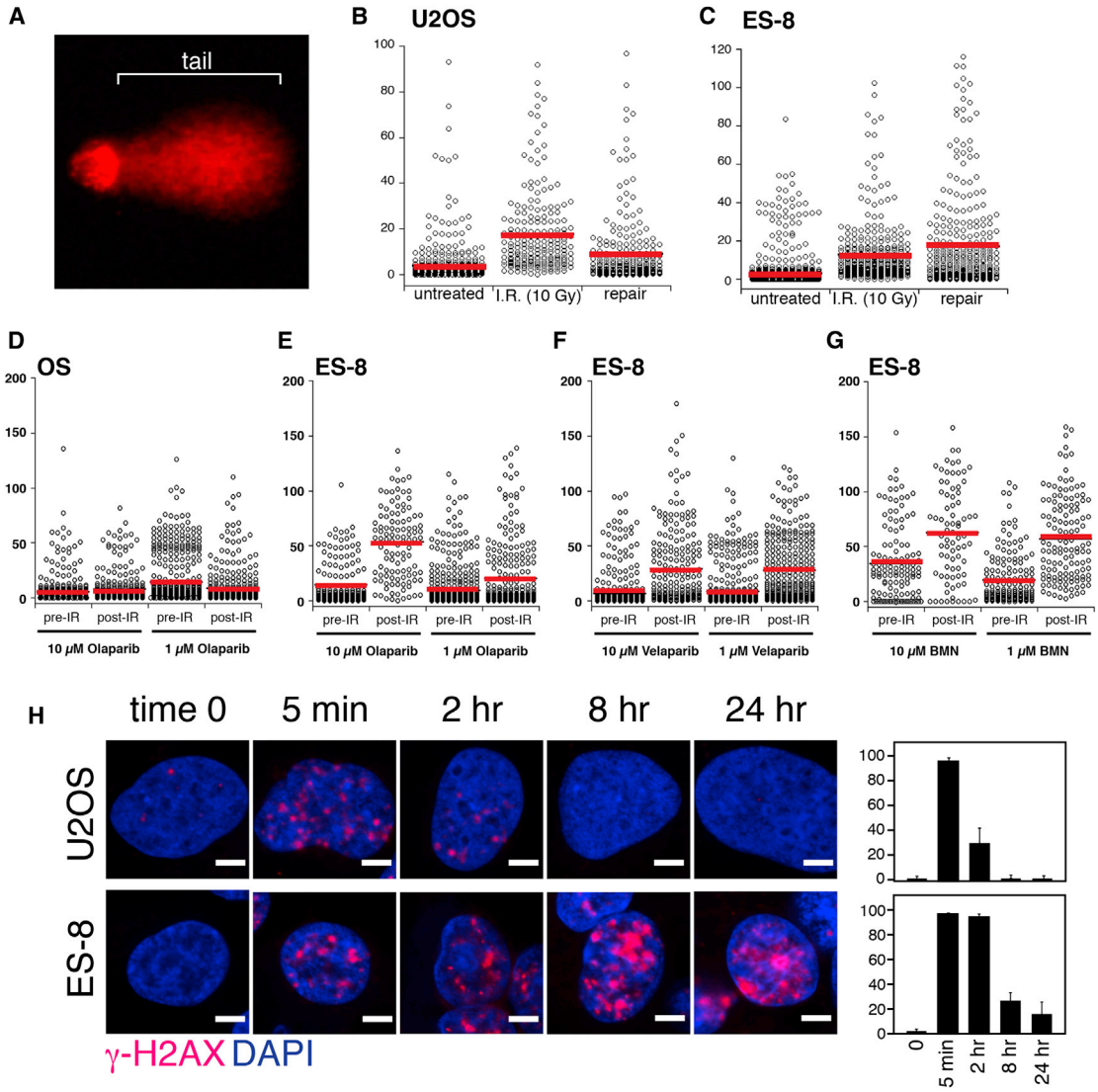

Figure 1. EWS Cell Lines Are Defective in dsDNA Break Repair

(A) Representative image of single-cell alkali electrophoresis with genomic DNA is shown in red; the tail moment is indicated.

(B and C) Comet data for U2OS cells (B) or ES-8 cells (C) prior to exposure to 10 Gy IR (untreated), 30 min after treatment, or 11 hr after treatment. The red line indicates the mean.

(D–G) Comet data for cells treated with 1 or 10 μM $PARP_i$ before and 12 hr after exposure to 10 Gy IR.

(H) Micrographs of U2OS and ES-8 nuclei (blue) stained for γ-H2AX (red). Scale bars, 1 μm. The proportion of γ-H2AX$^+$ cells (>20 foci/nucleus) are shown in the histograms to the right of the micrographs. Each bar represents the mean ± SD of duplicate scoring.

Tumor growth surrounding the femur (Figure 3N) and tumor histology (Figures 3O and 3P) of the orthotopic tumors were very similar to EWS tumors in patients.

In Vivo PK and PD of Veliparib, Olaparib, and BMN-673

To determine the murine equivalent dose (MED) and the level of tumor penetration of the three $PARP_i$s, we measured drug concentration in the plasma and tumors of CD1-nude mice with orthotopic xenografts at time points ranging from 30 min to 24 hr (Figure S3). We estimated the plasma area under the concentration-time curve (AUC) for each drug and compared those data to the AUC from plasma PK data in patients (Figure S3; Supplemental Information). Our data suggest that the most appropriate dose for twice-daily oral administration in mice is 12.5 mg/kg veliparib, 50 mg/kg olaparib, and 0.125 mg/kg BMN-673 (Supplemental Information). At 12 hr after dosing, concentration of at least 0.05 μM veliparib, 0.09 μM olaparib, and 0.015 μM BMN-673 were achieved in the orthotopic tumor (Figure S3).

Next, we combined the in vivo tumor pharmacokinetic data with the cytotoxicity data for each $PARP_i$ in combination with SN-38 or TMZ using a modified response surface model (RSM) approach (Figure S3; Supplemental Information). A total of seven

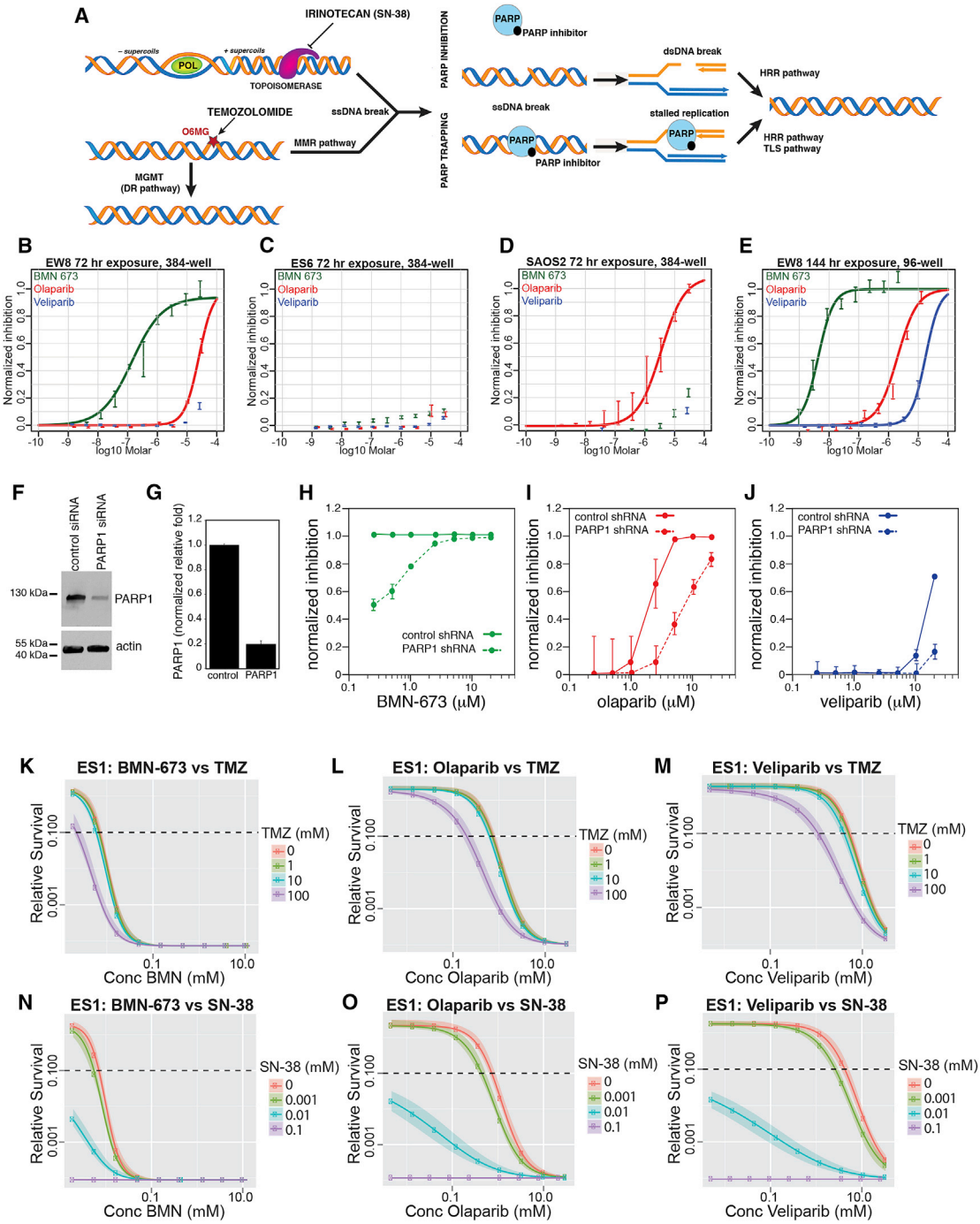

Figure 2. Potentiation of PARP$_i$ Cytotoxicity with IRN and TMZ

(A) Model of DNA damage and synthetic lethality for the combination of PARP$_i$s with TMZ or IRN.

(B–D) Dose response for EW-8, ES-6, and SAOS cells 72 hr after exposure to each indicated PARP$_i$. Curves fit using data pooled from two biological replicates, each with at least three technical replicates.

(E) A similar experiment was performed at 144 hr.

(F and G) (F) Immunoblot with quantification (G) of the knockdown of PARP1 in EW-8 cells transfected with a PARP1 siRNA.

(H–J) Dose response for BMN-673, olaparib, and veliparib in EW-8 cells at 72 hr with (solid line) and without (dashed line) knockdown of PARP1. Each data point is the mean ± SD of triplicate wells.

(K–P) Potentiation of PARP$_i$ in the presence of increasing concentrations of TMZ and SN-38. Curves were generated by taking horizontal slices through the efficacy surface estimated using the response surface model (RSM) approach.

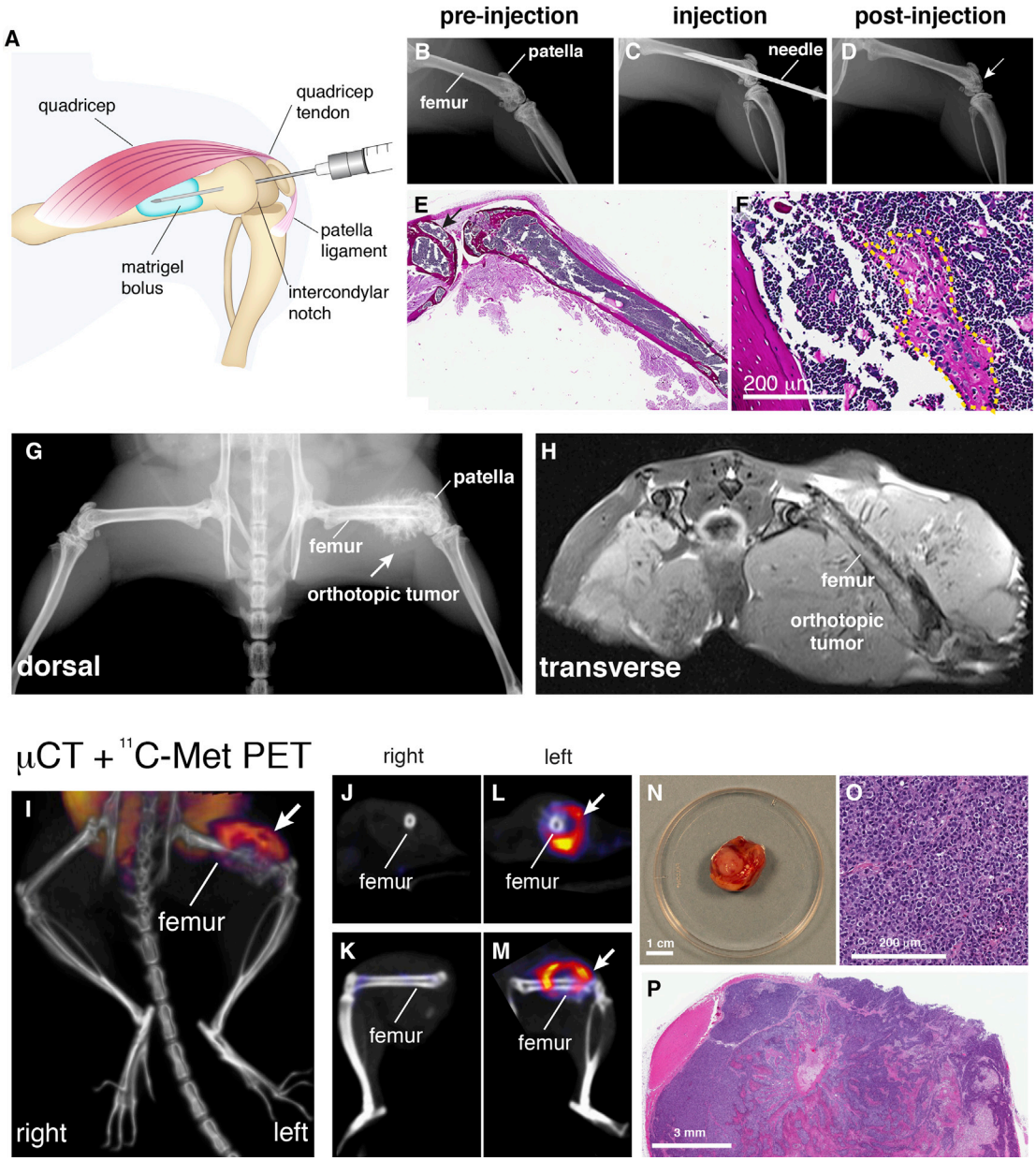

Figure 3. Development and Characterization of an Orthotopic EWS Tumor Model

(A) Diagram of the injection procedure.

(B–D) X-ray images of a mouse leg showing the injection procedure before, during, and after injection.

(E and F) Hematoxylin and eosin staining of mouse femur and bone marrow after injection of EWS cells in Matrigel (yellow dashed line). Arrows indicates the injection site.

(G) X-ray image of an orthotopic tumor with bony extensions (arrow).

(H) Transverse view of the soft-tissue and bony component of the orthotopic EWS xenograft in an MRI.

(I–M) Micro-PET/computed tomography (CT) scans using ^{11}C-methionine. The tumor (arrow) shows accumulation of the radiotracer.

(N) Photograph of the femur removed from a mouse with a large mass from the orthotopic xenograft.

(O and P) High- and low-power images of the orthotopic tumor showing its extension from the bone to the surrounding soft tissue.

drug pairs were examined (three $PARP_i$ + SN-38, three $PARP_i$ + TMZ, and SN-38 + TMZ) in four EWS cell lines. We used nonlinear regression to fit the observed 2D assay response surface as a function of the hill equation parameters for each compound, the overall efficacy, and kappa (κ), a measure of the interaction between the two drugs ($\kappa < 0$ indicates antagonism, $\kappa = 0$ indicates Loewe additivity, and $\kappa > 0$ indicates synergy). In every EWS cell line tested, the fitted κ value indicated additivity or

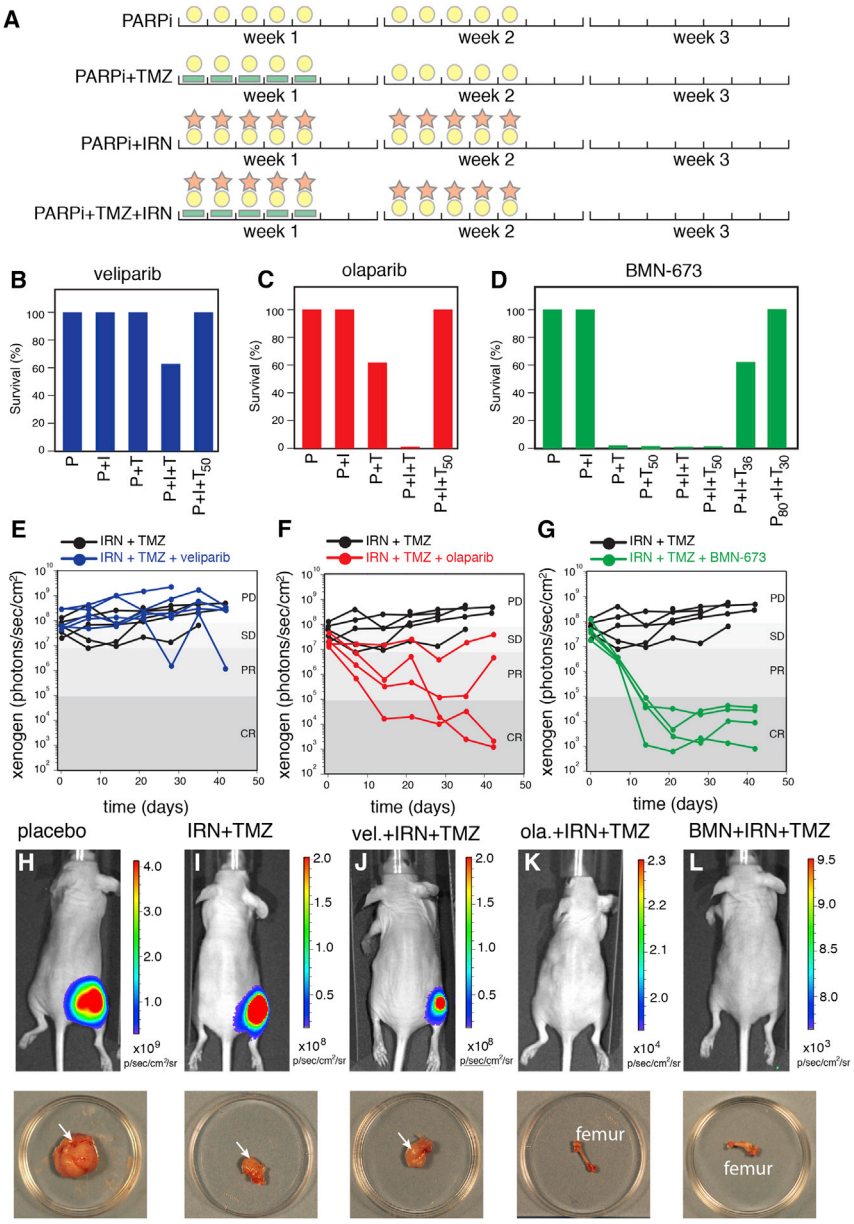

Figure 4. Preclinical Phase I/II Studies

(A) Drug-combination schedules. Yellow circles represent the $PARP_i$, green bars represent the TMZ and red stars represent daily IP dosing of IRN.

(B–D) Survival of mice in the preclinical phase I trial of each $PARP_i$ combined with IRN (I) or TMZ (T). In some groups, TMZ was reduced by 50% (T_{50}), 64% (T_{36}), or 70% (T_{30}). For BMN-673, the dose was reduced by 20% in one group (P_{80}).

(E–G) Preclinical phase II data for IRN + TMZ alone or in combination with veliparib (blue), olaparib (red), or BMN-673 (green). Tumor burden was monitored by Xenogen imaging.

(H–L) Representative Xenogen images for each treatment group and photographs of the tumors (arrows) or femurs at the end of the study.

synergy for all $PARP_i$ + SN-38 or TMZ combinations. Overall, the RSM analyses suggest that combining $PARP_i$ with either TMZ or SN-38 will be synergistic in EWS cell lines, with a greater degree of synergy observed for $PARP_i$ + TMZ drug pairs.

Although the sign and magnitude of the interaction between drug pairs is important, the combined efficacy at physiologically reasonable concentrations is more relevant when determining the potential utility of a drug combination for in vivo application. Using the RSM, one can predict the combined efficacy of a drug combination at any concentration. In translocation-positive EWS cell lines, SN-38 begins to significantly potentiate $PARP_i$ between 1 and 10 nM, whereas 10–100 μM TMZ is required for the same level of potentiation (Figures 2K–2P). In all translocation-positive EWS cell lines, we predict that the most efficacious drug combinations are: BMN 673 + SN-38 > Olaparib + SN-38 > BMN 673 + TMZ > all other drug pairs. In summary, our in vitro synergy study using RSM suggests that, although $PARP_i$ + TMZ pairs tend to be more synergistic than $PARP_i$ + SN-38 pairs, less SN-38 is needed to achieve a desirable level of efficacy.

To verify that the drugs penetrated the tumor and inhibited PARP in the tumor cells in vivo, we performed a PD assay II (Supplemental Information). At the MED, each of the $PARP_i$s reduced PARP activity within 1 hr, and PARP activity was restored over the next 6–12 hr (Figure S3). BMN-673 and olaparib sustained PARP inhibition longer than did veliparib in vivo.

Preclinical Phase I Study

Having established that sufficient levels of the three $PARP_i$s can be achieved in the orthotopic xenograft in vivo to inhibit PARP at the MED, we initiated a preclinical phase I trial to test the tolerability of $PARP_i$s as single agents and in combination with IRN, TMZ, or both. Our preclinical phase I trials were performed in three to five female CD1-nude mice per treatment group for a total of four to six courses of therapy (12–18 weeks; Figure 4A). The $PARP_i$s were administered orally twice daily to match the dosing in patients. Importantly, we used a low-dose, protracted schedule of IRN (i.e., 1.25 mg/kg twice daily for 5 days (d × 5 × 2) equivalent to 20 mg/m^2 d × 5 × 2 in children (Furman et al., 1999; Supplemental Information). The pediatric dose using this d × 5 × 2 schedule is much lower than that used in adults with cancer, who receive 100–350 mg/m^2 IRN one to three times per course (Kummar et al., 2011; Samol et al., 2012). TMZ was initially administered at 33 mg/kg on a d × 5 schedule, which is equivalent to 100 mg/m^2 in children (Horton et al., 2007).

For veliparib, nearly all combinations were well tolerated for four courses (12 weeks), except the veliparib + IRN + TMZ

combination (Figure 4B). In patients who do not tolerate the combination of TMZ + IRN, the dose is often reduced 50% from 100 mg/m^2 to 50 mg/m^2 (Wagner et al., 2009). Veliparib + IRN + TMZ (50%) was well tolerated for four courses (Figure 4B). Similar results were obtained with olaparib (Figure 4C). The tolerability of TMZ was even less in combination with BMN-673 (Figure 4D). The TMZ dose had to be reduced by 70% (10 mg/kg in mice and 30 mg/m^2 in children), and the BMN-673 dose by 20% of the MED (0.1 mg/kg) to make this combination tolerable (Figure 4D; Table S3).

Preclinical Phase II Study

To test if any of the PARP$_i$s reduce orthotopic EWS tumor growth in vivo, we performed a preclinical phase II study. Phase II studies are designed to provide rapid efficacy data by using a randomized, placebo-controlled study design (Supplemental Information).

Five groups comprising five mice per group with EW-8 orthotopic xenografts were used in this study. In addition to the placebo group, we included IRN + TMZ (50%) as a control group. The placebo group showed rapid tumor progression, and all mice were off study by 14 days after enrollment (data not shown). The mice in the IRN + TMZ (50%) group had stable disease (SD) or progressive disease (PD) but no partial response (PR) or complete response (CR) (Figures 4E–4G; Supplemental Information). The veliparib + IRN + TMZ (50%) group included 1 mouse with PR; the rest had SD or PD (Figure 4E). The olaparib + IRN + TMZ (50%) group had two mice with CR, one with PR, and one with SD (Figure 4F). The BMN-673 (80%) + IRN + TMZ (30%) group had four mice with CR (Figure 4G). Overall, the bioluminescence from the Xenogen imaging correlated with tumor weight and histopathologic evaluation (Figures 4H–4L and S4; Supplemental Information). As long as 12 weeks after cessation of treatment, mice with a CR that received olaparib + IRN + TMZ (50%) or BMN-673 (80%) + IRN + TMZ (30%) have no evidence of tumor recurrence, but those with PD, SD, or PR have all progressed rapidly (data not shown). ES-1 cells had poor engraftment and IRN + TMZ completely eliminated the tumors (data not shown). Mice with orthotopic ES-8 xenografted cells had similar response to the EW-8 cells (Figure S5). The ES-6 cells were similar to ES-1 in their poor engraftment efficiency and slow growth but the tumors showed response to olaparib + IRN + TMZ (50%) and BMN-673 (80%) + IRN + TMZ (50%) (Figure S5).

The C_{max} and AUC of SN-38 in mouse plasma has been reported to be slightly higher than those in human plasma because mice have higher levels of the plasma carboxylesterases that convert IRN to SN-38 (Morton et al., 2000, 2005). To determine whether the efficacy of IRN + PARP$_i$s in vivo was caused by the higher C_{max} or AUC of SN-38 in mice, we performed plasma PK and efficacy studies in carboxylesterase-deficient mice that more closely recapitulate the PK profile of SN-38 in humans (Morton et al., 2005). As shown previously, the plasma SN-38 C_{max} and AUC were slightly reduced in the carboxylesterase-deficient mice after intraperitoneal injection of IRN (Figure S5; Supplemental Information), but there was no effect on tumor response (Figure S5).

Preclinical Phase III Study

Our in vitro RSM predicted that BMN-673 + IRN or BMN-673 + TMZ would be significantly cytotoxic, olaparib + IRN may be more efficacious than olaparib + TMZ, and that veliparib-combination chemotherapy would probably not achieve significant in vivo efficacy at the dose and schedule used for these experiments. To test these predictions and directly compare the efficacy of each PARP$_i$ in combination with TMZ, IRN, or both, we performed a double-blind, randomized, placebo-controlled preclinical phase III trial. Briefly, we performed 350 intrafemoral injections of luciferase-labeled ES-8 cells into female CD1-nude mice. Over 5 weeks, the trial enrolled 274 mice and randomized them to 15 treatment groups (Table S4). Ten mice each were assigned to the placebo and single-agent PARPi groups; 25 mice were assigned to the BMN-673 (80%) + IRN + TMZ (30%) group; and 20 mice each were assigned to the other treatment groups (Table S4). All mice were assigned a mouse medical record number at enrollment, which allowed their data to be linked via an OpenClinica database (Supplemental Information).

Overall survival of mice in the placebo group did not significantly differ from that in the single-agent PARP$_i$-treatment groups (Figure 5A). As predicted by the RSM, of the groups that received combinations of PARP$_i$s with TMZ, only those that received BMN-673 + TMZ (50%) had significantly improved overall survival ($p = 0.0004$, Figure 5B). The groups that received PARP$_i$ + IRN tolerated the combinations well; responses were significantly better in the olaparib + IRN or BMN-673 + IRN groups than in the veliparib + IRN or TMZ + IRN groups ($p = 0.0001$, Figure 5C). All but one mouse in the olaparib + IRN + TMZ (50%) or BMN-673 (80%) + IRN + TMZ (30%) groups were alive at the end of the 12 week study (Figure 5D). All mice that came off study due to tumor growth were classified as having PD. Those that completed the four courses of therapy were classified as having CR, PR, SD, or PD based on the Xenogen thresholds used in the preclinical phase II study. The following percentages of each group showed CR: 15% (3/20) in the veliparib + IRN + TMZ (50%) group, 71% (12/17) in the olaparib + IRN + TMZ (50%) group, and 88% (14/16) in the BMN-673 (80%) + IRN + TMZ (30%) group. The Xenogen data correlated with tumor burden and histopathology (Figures 5I–5K).

In cell culture, IRN and TMZ showed strong potentiation of veliparib-mediated killing of EWS cells (Table S2). However, at the MED of that used in pediatric brain tumor phase II studies of veliparib with temozolomide (Su et al., 2014), our model predicted and our preclinical phase II and III studies validated that the levels of veliparib in the tumors were not sufficient to achieve high rates of CR. The pediatric brain tumor combination phase I trial with veliparib and temozolomide was designed to maximize the temozolomide dose and escalate the veliparib. However, our data presented here suggest that the opposite may be advantageous for Ewing sarcoma. Therefore, we performed additional phase I/II studies with a higher dose of veliparib (62.5 mg/kg twice a day ×5 ×2) in combination with IRN and TMZ (50%). The higher dose veliparib was well tolerated in combination with IRN and TMZ and had efficacy similar to that of olaparib + IRN + TMZ (50%) and BMN-673 + IRN + TMZ (30%) (Figure S5).

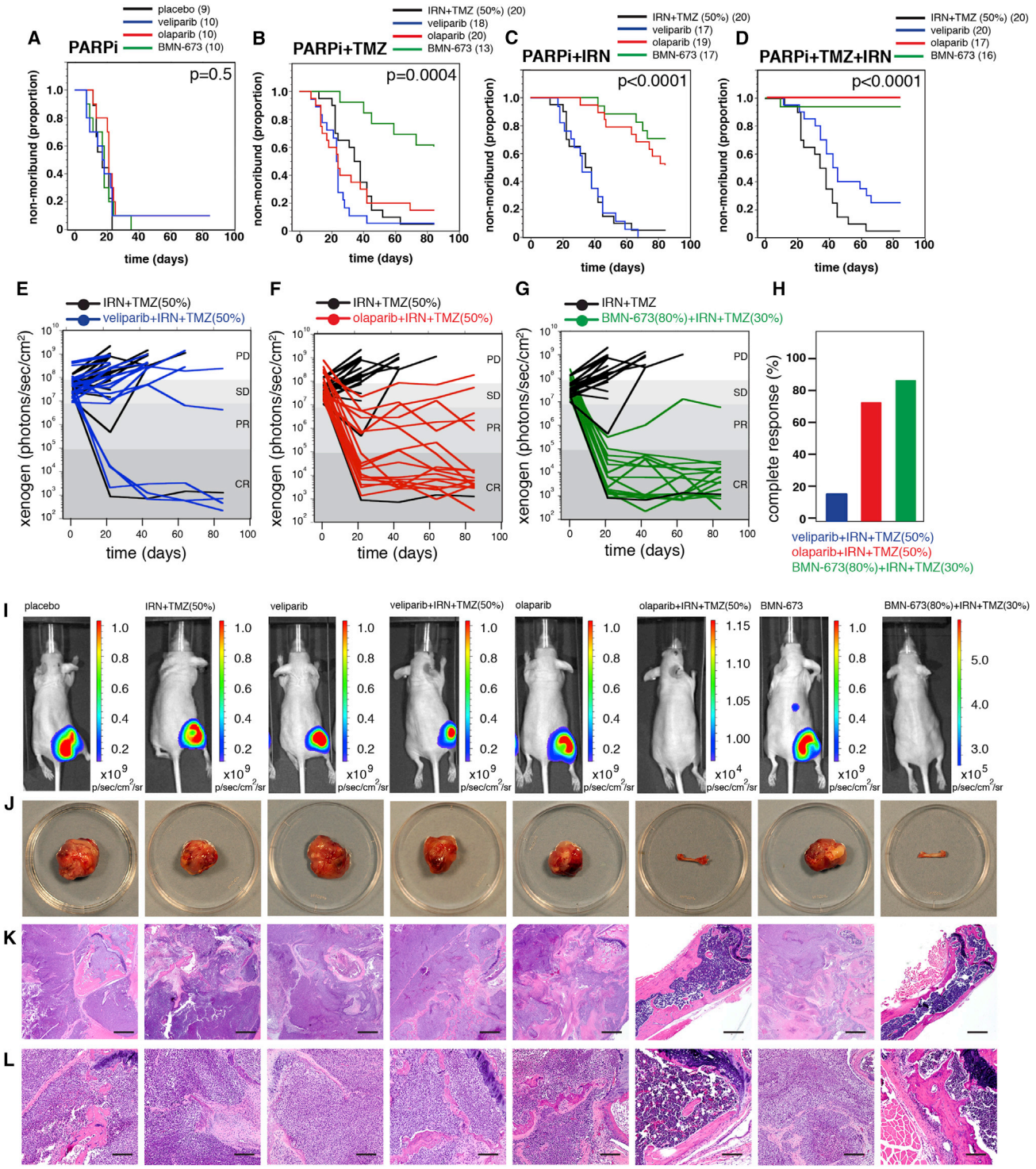

Figure 5. Preclinical Phase III Study

(A–D) Survival curves for each of the 15 treatment groups.

(E–G) Tumor response for individual mice in the TMZ + IRN group and the triple-drug combinations for veliparib (blue), olaparib (red), and BMN-67e (green). The cutoffs for progressive disease (PD), stable disease (SD), partial response (PR), and complete response (CR) are indicated by gray shading.

(H) Histogram of the proportion of CRs seen in each triple-drug treatment group.

(legend continued on next page)

DISCUSSION

Three PARP$_i$s in combination with DNA-damaging agents showed that PARP$_i$-mediated cytotoxicity can be potentiated by IRN and TMZ in vitro and in vivo. In vivo PK of veliparib, olaparib, and BMN-673 in plasma and tumor were used to calculate the MEDs and demonstrate tumor penetration and PARP inhibition at clinically relevant doses in orthotopic EWS xenografts. A preclinical phase I study revealed that combinations of PARP$_i$s with IRN were better tolerated than those with TMZ. Furthermore, the low-dose, protracted schedule of IRN used to treat pediatric patients with solid tumors (20 mg/m^2 d ×5 ×2) was well tolerated with all three PARP$_i$s, but the TMZ dose had to be reduced (50%–70%). The levels of all three PARP$_i$s in the tumor were sufficient to potentiate cytotoxicity with DNA-damaging agents but were insufficient to induce cytotoxicity on their own.

A preclinical phase II study demonstrated the efficacy of all three PARP$_i$s in combination with IRN and TMZ, and this provided justification for a subsequent in vivo efficacy study. In a double-blind, randomized, placebo-controlled preclinical phase III trial, we found significant improvement in overall survival and outcome when olaparib or BMN-673 was combined with TMZ and IRN. Most of the mice had a CR and did not exhibit tumor recurrence as long as 12 weeks after cessation of therapy. These data suggest that the combination of PARP$_i$s and IRN administered in the low-dose, protracted schedule optimized for pediatric patients should be considered for clinical development. A reduced dose of TMZ may be incorporated to provide full potentiation of PARP inhibition in EWS. Although veliparib was not as active as olaparib and BMN-673 in the preclinical phase III study, a higher dose of veliparib was well tolerated in preclinical phase I and had efficacy comparable to olaparib and BMN-673 in a preclinical phase II with IRN and TMZ.

DNA-Damaging Agents and PARP$_i$s in EWS

EWS cells express high levels of *SLFN11* and *PARP1* compared to other cancers, providing a rationale for combining DNA-damaging agents and PARP$_i$s. TMZ has been favored in the PARP$_i$ EWS clinical trials developed to date because in adults, camptothecins (topotecan or IRN) caused dose-limiting myelosuppression and diarrhea when combined with PARP$_i$s (Kummar et al., 2011; Samol et al., 2012). However, the low-dose, protracted schedule and the sensitivity of EWS cells to IRN make this camptothecin an attractive agent to combine with PARP$_i$s. Our PK, PD, and in vitro drug-combination studies showed that concentrations of PARP$_i$s and IRN can be achieved in vivo at levels sufficient to potentiate PARP-mediated cytotoxicity in vivo.

We did not test ionizing radiation in our studies, but this is another therapy that should be considered in combination with PARP$_i$s and DNA-damaging agents. EWS tumors are sensitive to IR, and similar potentiation might be achieved with IR in vivo (Lee et al., 2013). The majority of EWS cell lines have *TP53* mutations (Tirode et al., 2014), so it is difficult to compare the sensitivity of wild-type and *TP53*-deficient EWS cell lines to PARP$_i$s and DNA-damaging agents. However, *TP53*-deficient osteosarcoma cell lines are insensitive to those drug combinations, so p53 status alone cannot explain the sensitivity to PARP$_i$s and DNA-damaging agents in our study. Indeed, Oplustilova and colleagues found that PARP$_i$s can sensitize cells to camptothecin or ionizing radiation independent of p53 status in colorectal carcinoma cells (Oplustilova et al., 2012).

Our results suggest that STAG2 status does not correlate with sensitivity to DNA-damaging agents or PARP$_i$s in EWS, and this has important clinical consequences. In a separate whole-genome sequencing study, 17% of EWS tumors had inactivating somatic mutations in *STAG2*, a component of the cohesin complex (Tirode et al., 2014). Those data are consistent with previously published data from Solomon et al. showing that STAG2 is frequently lost in EWS (Solomon et al., 2011). Although STAG2-deficient glioblastoma cells appear to be more sensitive to PARP$_i$s (Bailey et al., 2014), this does not appear to be the case in EWS. It is encouraging that the *TP53;STAG2*-deficient EWS lines remain sensitive to the drug combinations because those patients have the worst overall survival (Tirode et al., 2014).

PARP Trapping

Although it is unlikely that high PARP1 levels alone are sufficient for conferring sensitivity to PARP$_i$s—a DNA repair defect must also be present—we did observe that the in vitro sensitivity of PARP$_i$s in EWS correlated with PARP trapping potential (Murai et al., 2012, 2014). The apparent differences in PARP trapping may be the result of differences in drug retention times. Specifically, BMN-673 may be more active as a single agent because it remains bound to PARP1 longer than olaparib or veliparib, resulting in more persistent PARP-DNA adducts. This may also contribute to its reduced tolerability. The implications of these data are related to dosing of each PARPi: efficacy may be improved if veliparib is dosed at a higher intensity to overcome these differences in tumor clearance and ultimately retention of PARP-bound drug in the tumor cells. Indeed, our preclinical phase II study with high-dose veliparib + IRN + TMZ showed efficacy similar to that of BMN-673 and olaparib. Similarly, once-daily dosing of BMN-673 may be better tolerated than twice-daily dosing without affecting PARP inhibition and efficacy. Because PARP$_i$s are combined with DNA-damaging agents to treat patients, it will be essential to balance the dosing and schedule of the PARP$_i$s with DNA-damaging agents to achieve maximum efficacy and tolerability.

Preclinical Testing for Pediatric Solid Tumors

Survival of patients with recurrent or metastatic EWS is among the worst of pediatric cancers. More importantly, outcome has not been significantly improved in 20 years. This explains the enthusiasm for treating recurrent EWS with PARP$_i$s, once the original discovery showed that EWS cell lines are sensitive to

(I) Representative Xenogen images of single-agent PARP$_i$s and corresponding triple-drug treatment groups.
(J) Representative photographs of tumors from placebo, IRN + TMZ, single-agent PARP$_i$ groups, and corresponding triple-drug treatment groups.
(K and L) Representative micrographs of hematoxylin-and-eosin-stained tissue sections from placebo, IRN + TMZ, single-agent PARP$_i$ groups, and corresponding triple-drug treatment groups. Scale bars in (K), 500 μm, and in (L), 100 μm.

olaparib (Garnett et al., 2012). Indeed, the first clinical trial (NCT01583543) opened within a month of that publication. However, several unanswered questions from that first study had important implications for the clinical trial. Could the levels of olaparib required to kill EWS cell lines in vitro be achieved in a patient's tumor in vivo? Could the $PARP_i$ be combined with a DNA-damaging agent? Which DNA-damaging agent should be used? What is the best dose and schedule for the $PARP_i$ and the DNA-damaging agent?

In this study, we developed and optimized a comprehensive preclinical-testing paradigm to answer these questions in EWS. The advantage of the program presented here is that it directly relates in vivo PK and PD to cytotoxicity in vitro and then uses MEDs and schedules to test those predictions in an array of systems (i.e., cell culture to relevant orthotopic EWS xenografts). Also, our preclinical phase I, II, and III trials mirror the approach used in clinical trials and provide an efficient system to advance new therapies. However, the key of any preclinical-testing effort is the predictive power of the preclinical results. The data presented here predict that single-agent olaparib will not be an effective treatment of EWS, and the efficacy of olaparib + TMZ may be limited by tolerability. As the ongoing trials with BMN-673 accrue patients, we will have additional opportunities to determine the predictive power of our preclinical-testing efforts.

The drug combination results from this study, specifically the utility of individual $PARP_i$, should not be generalized to non-EWS tumors in part because of the sensitivity of EWS cell lines to IRN (Barretina et al., 2012). Also, in vivo drug efficacy is the product of a multitude of effects beyond intrinsic cell sensitivity, such as influence of the tumor niche, immune system, and pharmacokinetics. Future efforts should focus on primary human orthotopic xenografts to complement the EWS cell line data presented here.

EXPERIMENTAL PROCEDURES

Comet Assay

Fifty thousand ES-1, ES- 6, ES-8, or U2OS cells or 100,000 mesenchymal stem cells were plated onto 12-well dishes per well. Cells were incubated for 24 hr and then treated with Parp inhibitor: 10 μM BMN-673, 1 μM BMN-673, 10 μM Veliparib, 1 μM Veliparib, 10 μM Oliparib, 1 μM Oliparib, or DMSO. Cells were incubated with the inhibitor for 14 hr and then treated with 10 Gy IR or were left untreated. Cells were incubated an additional 10 hr and then trypsinized and collected. For unrepaired control, cells were treated 10 Gy IR and immediately harvested. Fifty thousand cells were suspended in 30 μl PBS. Ten microliters of this suspension was mixed with 200 μl of 0.5% low melting point agarose (Sigma) and layered on CometSlides (Trevigen). Alkaline single-cell gel electrophoresis was performed as described previously (Benavente et al., 2013).

Animals

CD-1 nude immunodeficient mice were purchased from Charles River (strain code 087, heterozygous). Esterase-deficient SCID mice were bred and obtained from Philip Potter (St. Jude Children's Research Hospital). This study was carried out in strict accordance with the recommendations in the Guide to Care and Use of Laboratory Animals of the NIH. The protocol was approved by the Institutional Animal Care and Use Committee at St. Jude Children's Research Hospital. All efforts were made to minimize suffering. All mice were bred and housed in accordance with approved IACUC protocols. Animals were housed on a 12:12 light cycle (light on 6 a.m. off 6 p.m.) and provided food and water ad libitum.

Drugs Used for In Vitro Studies

Veliparib was purchased from Selleck (S1004, CAS 912444-00-9), Olaparib was purchased from LC Labs (O-9201, CAS 763113-22-0), BMN-673 was purchased from Abmole (BMN673, 1207456-01-6), Temozolomide was purchased from Combi-Blocks (OR-2567, CAS 85622-93-1), and SN-38 was purchased from (CAS 86639-52-3). The purity of all compounds was confirmed to be $\geq$95% using LC/MS coupled with UVTWC/ELSD detection, and concentration was verified using CLND if nitrogen was present in the compound.

Gene Expression Array Analysis

Microarray assays of Ewing sarcoma tumor samples (GSE37371) were compared to osteosarcoma arrays (HGU133v2 Affymetrix arrays, M.A.D. unpublished data). The data were RMA normalized, evaluated for quality by PCA and, after outlier removal, statistically compared using the unequal variance t test in Partek Genomics Suite 6.6. Select data known to be associated with DNA repair were then evaluated.

qPCR Analysis

Real-time RT-PCR experiments were performed using the Applied Biosystems 7900HT Fast Real-Time PCR system and custom TaqMan Array Micro Fluidic Cards (Life Technologies). RNA was prepared using Trizol following manufacturer instructions (Life Technologies, 15596018). cDNA was synthesized using the High Capacity cDNA to RNA kit (Life Technologies, 4387406) per user instructions. Samples were analyzed in triplicate and normalized to ACTB2 expression levels.

Histology and Immunohistochemistry

Paraffin-embedded formalin-fixed EWS tumors were serially sectioned for routine hematoxylin and eosin staining. Immunostaining for histochemical analysis was done with Ki67 (ThermoShandon, cat. RM-9106) (dilution 1:200) using hematoxylin as a counterstain (1:10 dilution). Histology images were obtained using Aperio ImageScope (Leica Biosystems).

PARP1 Knockdown

Gene-specific siRNAs (mix of four sequences) for PARP1 (Thermo Scientific, L-006656-03-0005) were transfected into ES-8 cells using Libofectamine RNAiMAX Reagent (Invitrogen, 13778). Cells were harvested 48 hr posttransfection and lysed for western analysis to confirm knockdown of PARP1. Also, cells were harvested by trypsinization, seeded onto 96-well plates at a density of 5000 cells per well in 40 μl of media. Seventy-two hours after transfection, cells were treated with 0, 1, 2.5, 5, 10, 20, 50, or 100 μM Olaparib, Veliparib, or BMN-673 in triplicate for each condition. Seventy-two hours after addition of PARPi, cells were analyzed for cellular activity using Cell Titer Glo (Promega, G7570).

SUPPLEMENTAL INFORMATION

Supplemental Information includes Supplemental Experimental Procedures, five figures, and four tables and can be found with this article online at http://dx.doi.org/10.1016/j.celrep.2014.09.028.

ACKNOWLEDGMENTS

We thank Jieun Kim for assistance with PET-CT and MRI, Angela McArthur for editing the manuscript, Fred Krafcik for help with cell screening, and David Finkelstein for assistance with bioinformatics analysis. This work was supported, in part, by a grant from Abbvie. It was also supported by a grant from Cancer Center Support (CA21765) from the NCI, grants to M.A.D. from the NIH (EY014867 and EY018599 and CA168875), and the American Lebanese Syrian Associated Charities (ALSAC). M.A.D. was also supported by a grant from Alex's Lemonade Stand Foundation for Childhood Cancer and HHMI. Finally, we thank John and Andra Tully and the Tully Family Foundation for generous support of Pediatric Solid Tumor Research at St. Jude Children's Research Hospital.

Received: June 9, 2014
Revised: July 23, 2014
Accepted: September 19, 2014
Published: October 23, 2014

REFERENCES

Ashworth, A. (2008). A synthetic lethal therapeutic approach: poly(ADP) ribose polymerase inhibitors for the treatment of cancers deficient in DNA double-strand break repair. J. Clin. Oncol. *26*, 3785–3790.

Bagatell, R., London, W.B., Wagner, L.M., Voss, S.D., Stewart, C.F., Maris, J.M., Kretschmar, C., and Cohn, S.L. (2011). Phase II study of irinotecan and temozolomide in children with relapsed or refractory neuroblastoma: a Children's Oncology Group study. J. Clin. Oncol. *29*, 208–213.

Bailey, M.L., O'Neil, N.J., van Pel, D.M., Solomon, D.A., Waldman, T., and Hieter, P. (2014). Glioblastoma cells containing mutations in the cohesin component STAG2 are sensitive to PARP inhibition. Mol. Cancer Ther. *13*, 724–732.

Bajrami, I., Frankum, J.R., Konde, A., Miller, R.E., Rehman, F.L., Brough, R., Campbell, J., Sims, D., Rafiq, R., Hooper, S., et al. (2014). Genome-wide profiling of genetic synthetic lethality identifies CDK12 as a novel determinant of PARP1/2 inhibitor sensitivity. Cancer Res. *74*, 287–297.

Barretina, J., Caponigro, G., Stransky, N., Venkatesan, K., Margolin, A.A., Kim, S., Wilson, C.J., Lehár, J., Kryukov, G.V., Sonkin, D., et al. (2012). The Cancer Cell Line Encyclopedia enables predictive modelling of anticancer drug sensitivity. Nature *483*, 603–607.

Benavente, C.A., McEvoy, J.D., Finkelstein, D., Wei, L., Kang, G., Wang, Y.D., Neale, G., Ragsdale, S., Valentine, V., Bahrami, A., et al. (2013). Cross-species genomic and epigenomic landscape of retinoblastoma. Oncotarget *4*, 844–859.

Brenner, J.C., Feng, F.Y., Han, S., Patel, S., Goyal, S.V., Bou-Maroun, L.M., Liu, M., Lonigro, R., Prensner, J.R., Tomlins, S.A., and Chinnaiyan, A.M. (2012). PARP-1 inhibition as a targeted strategy to treat Ewing's sarcoma. Cancer Res. *72*, 1608–1613.

Bryant, H.E., Schultz, N., Thomas, H.D., Parker, K.M., Flower, D., Lopez, E., Kyle, S., Meuth, M., Curtin, N.J., and Helleday, T. (2005). Specific killing of BRCA2-deficient tumours with inhibitors of poly(ADP-ribose) polymerase. Nature *434*, 913–917.

Byers, L.A., Wang, J., Nilsson, M.B., Fujimoto, J., Saintigny, P., Yordy, J., Giri, U., Peyton, M., Fan, Y.H., Diao, L., et al. (2012). Proteomic profiling identifies dysregulated pathways in small cell lung cancer and novel therapeutic targets including PARP1. Cancer Discov. *2*, 798–811.

Casey, D.A., Wexler, L.H., Merchant, M.S., Chou, A.J., Merola, P.R., Price, A.P., and Meyers, P.A. (2009). Irinotecan and temozolomide for Ewing sarcoma: the Memorial Sloan-Kettering experience. Pediatr. Blood Cancer *53*, 1029–1034.

Delattre, O., Zucman, J., Plougastel, B., Desmaze, C., Melot, T., Peter, M., Kovar, H., Joubert, I., de Jong, P., Rouleau, G., et al. (1992). Gene fusion with an ETS DNA-binding domain caused by chromosome translocation in human tumours. Nature *359*, 162–165.

Farmer, H., McCabe, N., Lord, C.J., Tutt, A.N., Johnson, D.A., Richardson, T.B., Santarosa, M., Dillon, K.J., Hickson, I., Knights, C., et al. (2005). Targeting the DNA repair defect in BRCA mutant cells as a therapeutic strategy. Nature *434*, 917–921.

Fong, P.C., Boss, D.S., Yap, T.A., Tutt, A., Wu, P., Mergui-Roelvink, M., Mortimer, P., Swaisland, H., Lau, A., O'Connor, M.J., et al. (2009). Inhibition of poly(ADP-ribose) polymerase in tumors from BRCA mutation carriers. N. Engl. J. Med. *361*, 123–134.

Furman, W.L., Stewart, C.F., Poquette, C.A., Pratt, C.B., Santana, V.M., Zamboni, W.C., Bowman, L.C., Ma, M.K., Hoffer, F.A., Meyer, W.H., et al. (1999). Direct translation of a protracted irinotecan schedule from a xenograft model to a phase I trial in children. J. Clin. Oncol. *17*, 1815–1824.

Garnett, M.J., Edelman, E.J., Heidorn, S.J., Greenman, C.D., Dastur, A., Lau, K.W., Greninger, P., Thompson, I.R., Luo, X., Soares, J., et al. (2012). Systematic identification of genomic markers of drug sensitivity in cancer cells. Nature *483*, 570–575.

Granowetter, L., Womer, R., Devidas, M., Krailo, M., Wang, C., Bernstein, M., Marina, N., Leavey, P., Gebhardt, M., Healey, J., et al. (2009). Dose-intensified compared with standard chemotherapy for nonmetastatic Ewing sarcoma family of tumors: a Children's Oncology Group Study. J. Clin. Oncol. *27*, 2536–2541.

Horton, T.M., Thompson, P.A., Berg, S.L., Adamson, P.C., Ingle, A.M., Dolan, M.E., Delaney, S.M., Hedge, M., Weiss, H.L., Wu, M.F., and Blaney, S.M.; Children's Oncology Group Study (2007). Phase I pharmacokinetic and pharmacodynamic study of temozolomide in pediatric patients with refractory or recurrent leukemia: a Children's Oncology Group Study. J. Clin. Oncol. *25*, 4922–4928.

Howlader, N., Noone, A.M., Krapcho, M., Garshell, J., Neyman, N., Altekruse, S.F., Kosary, C.L., Yu, M., Ruhl, J., Tatalovich, Z., et al. (2013). SEER Cancer Statistics Review, 1975–2010, National Cancer Institute. Bethesda, MD, http://seer.cancer.gov/csr/1975_2011/, based on November 2013 SEER data submission, posted to the SEER web site, April 2014.

Hsiang, Y.H., Lihou, M.G., and Liu, L.F. (1989). Arrest of replication forks by drug-stabilized topoisomerase I-DNA cleavable complexes as a mechanism of cell killing by camptothecin. Cancer Res. *49*, 5077–5082.

Kummar, S., Chen, A., Ji, J., Zhang, Y., Reid, J.M., Ames, M., Jia, L., Weil, M., Speranza, G., Murgo, A.J., et al. (2011). Phase I study of PARP inhibitor ABT-888 in combination with topotecan in adults with refractory solid tumors and lymphomas. Cancer Res. *71*, 5626–5634.

Lee, H.J., Yoon, C., Schmidt, B., Park, J., Zhang, A.Y., Erkizan, H.V., Toretsky, J.A., Kirsch, D.G., and Yoon, S.S. (2013). Combining PARP-1 inhibition and radiation in Ewing sarcoma results in lethal DNA damage. Mol. Cancer Ther. *12*, 2591–2600.

Lessnick, S.L., and Ladanyi, M. (2012). Molecular pathogenesis of Ewing sarcoma: new therapeutic and transcriptional targets. Annu. Rev. Pathol. *7*, 145–159.

Morton, C.L., Wierdl, M., Oliver, L., Ma, M.K., Danks, M.K., Stewart, C.F., Eiseman, J.L., and Potter, P.M. (2000). Activation of CPT-11 in mice: identification and analysis of a highly effective plasma esterase. Cancer Res. *60*, 4206–4210.

Morton, C.L., Iacono, L., Hyatt, J.L., Taylor, K.R., Cheshire, P.J., Houghton, P.J., Danks, M.K., Stewart, C.F., and Potter, P.M. (2005). Activation and antitumor activity of CPT-11 in plasma esterase-deficient mice. Cancer Chemother. Pharmacol. *56*, 629–636.

Murai, J., Huang, S.Y., Das, B.B., Renaud, A., Zhang, Y., Doroshow, J.H., Ji, J., Takeda, S., and Pommier, Y. (2012). Trapping of PARP1 and PARP2 by Clinical PARP Inhibitors. Cancer Res. *72*, 5588–5599.

Murai, J., Huang, S.Y., Renaud, A., Zhang, Y., Ji, J., Takeda, S., Morris, J., Teicher, B., Doroshow, J.H., and Pommier, Y. (2014). Stereospecific PARP trapping by BMN 673 and comparison with olaparib and rucaparib. Mol. Cancer Ther. *13*, 433–443.

Oplustilova, L., Wolanin, K., Mistrik, M., Korinkova, G., Simkova, D., Bouchal, J., Lenobel, R., Bartkova, J., Lau, A., O'Connor, M.J., et al. (2012). Evaluation of candidate biomarkers to predict cancer cell sensitivity or resistance to PARP-1 inhibitor treatment. Cell Cycle *11*, 3837–3850.

Pettitt, S.J., Rehman, F.L., Bajrami, I., Brough, R., Wallberg, F., Kozarewa, I., Fenwick, K., Assiotis, I., Chen, L., Campbell, J., et al. (2013). A genetic screen using the PiggyBac transposon in haploid cells identifies Parp1 as a mediator of olaparib toxicity. PLoS One *8*, e61520.

Quiros, S., Roos, W.P., and Kaina, B. (2010). Processing of O6-methylguanine into DNA double-strand breaks requires two rounds of replication whereas apoptosis is also induced in subsequent cell cycles. Cell Cycle *9*, 168–178.

Samol, J., Ranson, M., Scott, E., Macpherson, E., Carmichael, J., Thomas, A., and Cassidy, J. (2012). Safety and tolerability of the poly(ADP-ribose) polymerase (PARP) inhibitor, olaparib (AZD2281) in combination with topotecan for the treatment of patients with advanced solid tumors: a phase I study. Invest. New Drugs *30*, 1493–1500.

Solomon, D.A., Kim, T., Diaz-Martinez, L.A., Fair, J., Elkahloun, A.G., Harris, B.T., Toretsky, J.A., Rosenberg, S.A., Shukla, N., Ladanyi, M., et al. (2011). Mutational inactivation of STAG2 causes aneuploidy in human cancer. Science *333*, 1039–1043.

Stahl, M., Ranft, A., Paulussen, M., Bölling, T., Vieth, V., Bielack, S., Görtitz, I., Braun-Munzinger, G., Hardes, J., Jürgens, H., and Dirksen, U. (2011). Risk of recurrence and survival after relapse in patients with Ewing sarcoma. Pediatr. Blood Cancer *57*, 549–553.

Su, J.M., Thompson, P., Adesina, A., Li, X.N., Kilburn, L., Onar-Thomas, A., Kocak, M., Chyla, B., McKeegan, E., Warren, K.E., et al. (2014). A phase I trial of veliparib (ABT-888) and temozolomide in children with recurrent CNS tumors: a Pediatric Brain Tumor Consortium report. Neuro Oncol., Published online June 7, 2014.

Tirode, F., Surdez, D., Ma, X., Parker, M., Le Deley, M.C., Bahrami, A., Zhang, Z., Lapouble, E., Grossetete-Lamali, S., Rusch, M., et al. (2014). Genomic landscape of Ewing sarcoma defines an aggressive subtype with co-association of STAG2 and TP53 mutations. Cancer Discov., Published online September 15, 2014.

Tutt, A.N., Lord, C.J., McCabe, N., Farmer, H., Turner, N., Martin, N.M., Jackson, S.P., Smith, G.C., and Ashworth, A. (2005). Exploiting the DNA repair defect in BRCA mutant cells in the design of new therapeutic strategies for cancer. Cold Spring Harb. Symp. Quant. Biol. *70*, 139–148.

Wagner, L.M., Villablanca, J.G., Stewart, C.F., Crews, K.R., Groshen, S., Reynolds, C.P., Park, J.R., Maris, J.M., Hawkins, R.A., Daldrup-Link, H.E., et al. (2009). Phase I trial of oral irinotecan and temozolomide for children with relapsed high-risk neuroblastoma: a new approach to neuroblastoma therapy consortium study. J. Clin. Oncol. *27*, 1290–1296.

Zoppoli, G., Regairaz, M., Leo, E., Reinhold, W.C., Varma, S., Ballestrero, A., Doroshow, J.H., and Pommier, Y. (2012). Putative DNA/RNA helicase Schlafen-11 (SLFN11) sensitizes cancer cells to DNA-damaging agents. Proc. Natl. Acad. Sci. USA *109*, 15030–15035.